Alexandria Engineering Journal (2018) 57, 3437–3450

HOSTED BY

Alexandria University

Alexandria Engineering Journal

www.elsevier.com/locate/aej
www.sciencedirect.com

ORIGINAL ARTICLE

Analytical and numerical investigations of the collapse of blood vessels with nonlinear wall material embedded in nonlinear soft tissues

Mohammed Ghazy [a,1], Mohamed B. Elgindi [b], Dongming Wei [c,*]

[a] KFUPM University, Saudi Arabia
[b] Texas A & M University-Qatar, Qatar
[c] Nazarbayev University, Kazakhstan

Received 14 June 2017; revised 5 January 2018; accepted 24 March 2018
Available online 22 November 2018

KEYWORDS

Blood vessel;
Bifurcation;
Critical buckling pressure;
Flow rates

Abstract In this paper, shapes of nonlinear blood vessels, surrounded by nonlinear soft tissues, and buckled due to radial pressure are solved for analytically and numerically. The blood flow rates through the bucked shapes are then computed numerically. A Fung-type isotropic hyperelastic stress-strain constitutive equation is used to establish a nonlinear mathematical model for radial buckling of blood vessels. The surrounding tissues are modeled as non-linear springs. Novel formulas for critical buckling pressures are derived analytically from the bifurcation analysis. This analysis shows that the nonlinearity of vessel's wall increases the critical buckling pressure. A numerical differential correction scheme is introduced to solve for post-buckling shapes. And the corresponding blood flow rates are provided before touching of the collapsed walls. The blood flow rate through a one-point wall-touching case is also provided. Numerical results show that both vessel's wall and soft tissues nonlinearities increase, locally, the flow rate through the buckled blood vessels. More importantly, a nonlinear relation between blood flow rate and the soft tissue spring constants is found.

1. Introduction

During surgery, due to loss of pressure, it is important to know the blood flow rates in various blood vessels corresponding to a given blood pressure difference between the exterior and the interior of the vessel [1]. This motivates the study of buckling and post-buckling behavior of blood vessels. And since conducting isolated blood vessels testing may lead to unidentified deformation state [2], analytical and numerical investigations of blood vessels deformation were found necessary. In [3],

* Corresponding author.
E-mail addresses: mohammed.ghazy@kfupm.edu.sa (M. Ghazy), mohamed.elgindi@qatar.tamu.edu (M.B. Elgindi), dongming.wei@nu.edu.kz (D. Wei).
[1] On leave from Alexandria University, Egypt.

Peer review under responsibility of Faculty of Engineering, Alexandria University.

https://doi.org/10.1016/j.aej.2018.03.002

post-buckling cross sectional shapes of embedded vessels with linear wall material and supporting tissues are considered. Flow rates through these vessels are calculated when acted upon by uniform pressure for various deformed shapes. In an interesting case, the post-buckling of free blood vessels with opposite sides in contact is considered in [4,5]. In [6,7] it is shown how understanding the collapse of veins helped explaining the blood circulation in giraffe where changing the position of the head produces a large difference in the potential energy. Bent axial buckling of blood vessels has also been studied extensively in [8]. In all the previous studies, Hooke's law has been used to model vessels' walls' deformations and the blood was treated as Newtonian fluids. It is well known that blood vessels walls as well as blood respond in a nonlinear fashion to applied forces at larger ranges of strains and stresses [9–15]. Post buckling shapes of nonlinear wall vessels with nonlinear soft tissues are calculated numerically in [16]. For a comprehensive survey of the current literature on artery buckling the reader is referred to [17].

In the current research we assume that the flow of the blood through the vessel is slow and steady and the cross section does not vary much along an axial segment, so that the internal pressure may be taken, locally, as constant. We also assume the blood to be a Newtonian fluid, which is adequate for blood flows in large vessels. Some researches considered the pulsating nature of the blood in the arteries [18–20], by taking the pressure to be periodic. The pulsating nature of blood as well as the hydrodynamic properties pertinent to its non-Newtonian turbulent flow are out of the scope of this paper. Based on the current assumptions, the deformed shapes can be solved for first. Then the flow rates can be determined accordingly.

Nonlinear models for the blood vessel's wall and the surrounding soft tissues are used in the current studies. These nonlinearities are expected to affect the post-buckling shapes and consequently the flow rates through them. Therefore, the results of our study will represent a useful step in describing blood vessels deformations more precisely, due to the use of the more general Fung-type stress strain constitutive equation, compared with the results using Hooke's law.

We extend and complete the preliminary results reported in [16] by recasting the vector form of the equilibrium equation in a single nonlinear scalar equation, namely Eq. (16) Section 2, from which we provide a detail bifurcation analysis of the problem. In addition to computing the deformed shapes of the cross-section of the buckled blood vessel, we also compute various blood flow rates through these deformed cross-sections using experimental data from literature. In this paper a detailed bifurcation analysis based on the model in [16] is introduced, and the post-buckling shapes obtained numerically there in are used to calculate the blood flow rate. In Section 2, we review the formulation of the equilibrium equations. In Section 3, we present a bifurcation analysis of the equilibrium equations leading to explicit formulas for the bifurcation points and the corresponding first order bifurcation solutions. Then we explain how the nonlinearity of the blood vessel affect the critical buckling pressure compared with the results which assume linear elastic walls. In Section 4, we present the numerical scheme used to obtain solutions to the post-buckling shapes of the blood vessel. In Section 5, we show the numerical results and calculate the blood flow rates through these buckled cross sections and discuss the results demonstrating in details the effect of vessel's wall and soft tissues nonlinearity on the blood flow. Finally, in Section 6, we give some concluding remarks.

2. Mathematical formulation

The following modified stress-strain ($\sigma - \epsilon$) model for the blood vessel's wall was used in [16]

$$\sigma = E\epsilon + \beta\alpha^2|\epsilon|\epsilon, \tag{1}$$

where β, α are material parameters and E is the Young's modulus. Eq. 1 is obtained from the well-known equation

$$\sigma = E\epsilon + \beta(e^{\alpha\epsilon} - 1 - \alpha\epsilon), \tag{2}$$

provided in [12], by taking Taylor expansion and keeping up to the quadratic term, when $\alpha\epsilon$ is sufficiently small. Experimental results show that $\alpha = 1.5, \beta = 90$ kPa and $E = 20$ kPa, for the range 20 kPa $< \sigma <$ 60 kPa, see e.g., [12]. For a complete survey of all the constitutive models for blood vessels, see [9].

It is well known that the soft tissues surrounding blood vessels play a major rule during the collapse of these vessels, [3,15]. In this paper the surrounding tissues are modeled as nonlinear springs governed by the generalized Hooke's law

$$F(s) = k_1 s + k_2 g(s), \tag{3}$$

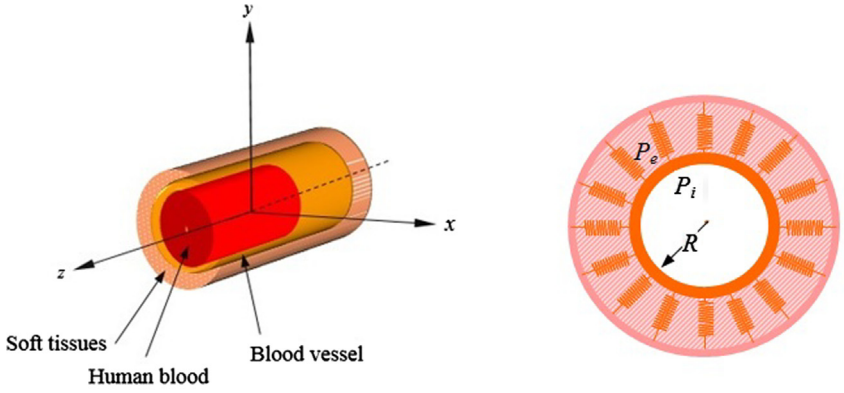

Fig. 1 a: A blood vessel surrounded by soft tissue, b: elastic cylinder tethered to a rigid cylinder.

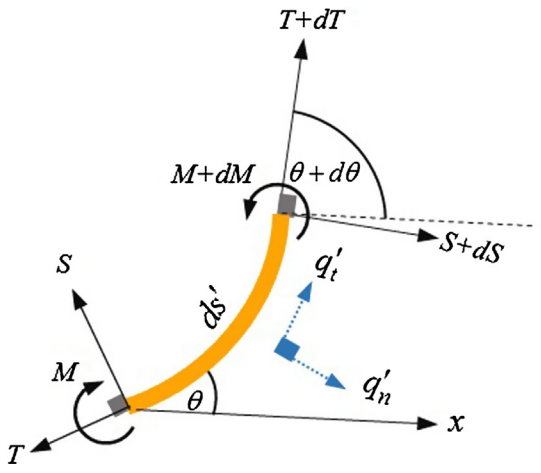

Fig. 2 An element length.

where k_1 and k_2 are positive constants, and $g(s)$ is an odd function of s. This formulation matches the behavior of some soft tissues observed using ultrasound indentation [21]. However, since our study is not specific to certain soft tissue, generic values for the constants k_1 and k_2 are assumed in our numerical calculations. These values will be chosen to show the effect of the nonlinearity of the soft tissue on the buckling shapes and blood flow rate.

Fig. 1 depicts a long thin-walled cylindrical blood vessel tethered by continuously distributed nonlinear springs to a rigid outer cylinder. The interior cylinder is subjected to internal pressure P_i and external pressure P_e. This cylinder will remain circular unless a critical or bifurcation pressure difference is exceeded.

2.1. Equilibrium equations

To formulate the mathematical equations governing the equilibrium, we consider the forces acting on an elemental length of the cross section of the interior cylinder. In Fig. 2, below, S is the shearing force, s' is the arc length, q'_t is the tangential stress per unit length, q'_n is the normal stress per unit length, M is the bending moment, T is the tensional force, and θ is the local angle the vessel wall makes with the x-axis.

From Fig. 2, if we assume a small element length, the equilibrium of forces in the normal and tangential directions respectively gives [3]

$$Td\theta = q'_n ds' + dS, \tag{4}$$

$$q'_t ds' + Sd\theta + dT = 0, \tag{5}$$

while balance of moments gives

$$dM = Sds'. \tag{6}$$

Eqs. (4)–(6) are the basic equilibrium equations as in [3]. In Fig. 2, the wall thickness is assumed to be sufficiently small compared to the radius. If we substitute the relation between bending moment and stress, i.e. $\sigma I_1 = M\epsilon\frac{ds'}{d\theta}$, into the stress-strain Eq. (1), the bending moment can then be expressed as

$$M = EI_1\frac{d\theta}{ds'} + \beta\alpha^2 I_2\left|\frac{d\theta}{ds'}\right|\frac{d\theta}{ds'}, \tag{7}$$

where I_1 and I_2 are the first and the second area moment of inertia respectively. Substituting (7) into (6), the shear force can be written as

$$S = \frac{dM}{ds'} = EI_1\frac{d^2\theta}{ds'^2} + 2\beta\alpha^2 I_2\left|\frac{d\theta}{ds'}\right|\frac{d^2\theta}{ds'^2}. \tag{8}$$

Dividing (5) by ds' and substituting from (8) we get

$$q'_t + \left(EI_1\frac{d^2\theta}{ds'^2} + 2\beta\alpha^2 I_2\left|\frac{d\theta}{ds'}\right|\frac{d^2\theta}{ds'^2}\right)\frac{d\theta}{ds'} + \frac{dT}{ds'} = 0. \tag{9}$$

Then dividing (4) by ds' and rewriting we get

$$T\frac{d\theta}{ds'} - \frac{dS}{ds'} = q'_n. \tag{10}$$

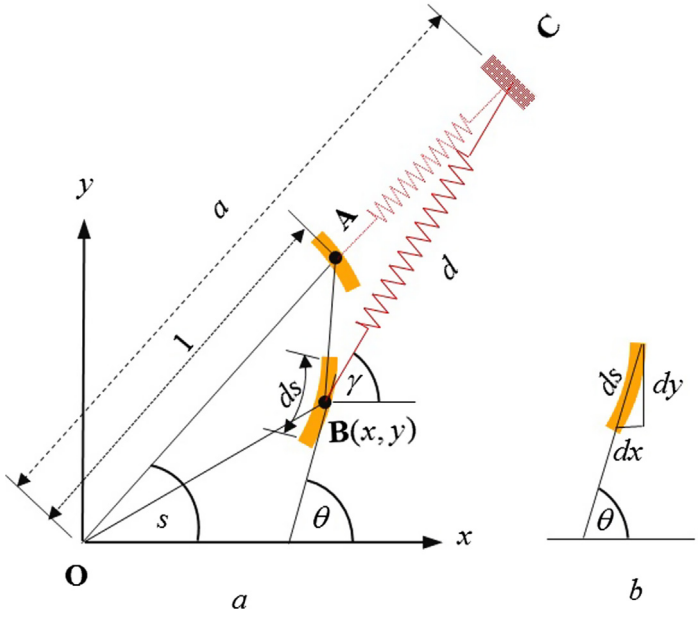

Fig. 3 a: Displacement from point A to point B, b: orientation of element length relative to coordinates at point B.

And, differentiating (10) with respect to ds' gives

$$\frac{dT}{ds'}\frac{d\theta}{ds'} + T\frac{d^2\theta}{ds'^2} - \frac{d^2S}{ds^2} = \frac{dq'_n}{ds'}. \tag{11}$$

Before proceeding to the final equation, we can simplify the derivation by using the following dimensionless variables

$$s = \frac{s'}{R}, \quad q_n = \frac{q'_n R^3}{EI_1}, \quad q_t = \frac{q'_t R^3}{EI_1}, \quad \hat{\beta} = \frac{2\beta\alpha^2 I_2}{EI_1 R}. \tag{12}$$

where, the undeformed radius R, and the quantity $\frac{EI_1}{R^2}$, which characterize the geometry and material properties, are used to normalize distances and forces respectively. From now on the prime ($'$) will be used to denote differentiation with respect to s i.e. $\theta' = \frac{d\theta}{ds}$. By applying (12) to (8), then differentiating with respect to s, we get

$$S' = \left(1 + \hat{\beta}|\theta'|\right)\theta''' + \hat{\beta} sign(\theta')(\theta'')^2. \tag{13}$$

Applying (12) to (10) then substituting from (13) we get

$$T\theta' = \theta''' + \hat{\beta}|\theta'|\theta''' + \hat{\beta} sign(\theta')(\theta'')^2 + q_n, \tag{14}$$

and again applying (12) to (9) we get

$$T' = -\left(1 + \hat{\beta}|\theta'|\right)\theta'\theta'' - q_t. \tag{15}$$

Finally, differentiating (13) with respect to s, then substituting it with (14) and (15) into (11) after normalizing it and multiplying by θ' gives

$$\begin{aligned}&\left[1 + \hat{\beta}|\theta'|\right]\theta'\theta'''' - \left[\theta'' + \hat{\beta}|\theta'|\theta'' - 3\hat{\beta}\theta' sign(\theta')\theta''\right]\theta''' \\ &+ \left[(\theta')^3 - q_n + \hat{\beta}|\theta'|(\theta')^3 - \hat{\beta} sign(\theta')\theta''^2 + 2\hat{\beta}\delta(\theta')\theta'\theta''^2\right]\theta'' \\ &+ q_t(\theta')^2 + q'_n\theta' = 0,\end{aligned} \tag{16}$$

where $\delta(.)$ denotes the *Dirac-Delta* function.

To solve the previous equation we still need some boundary conditions from the geometry of the deformation of the blood vessel's cross section. In Fig. 3, we demonstrate changes in the coordinates of the element length due to a displacement from point A on the initial circular shape to point B on a deformed shape. The origin of the xy coordinates is placed at the center of the local cross section, where the xy plane is perpendicular to the longitudinal axis of the vessel. The distance a from the origin to point **C**, at the far end of the soft tissue, is arbitrary. The distance $\mathbf{OA} = 1$ is the normalized undeformed radius, and the distance d from **B** to **C** is the current spring length.

In Fig. 3.a, x, y are the coordinates of point **B**. From Fig. 3. b, their derivatives are

$$x' = \cos\theta, \quad y' = \sin\theta. \tag{17}$$

It is obvious, from Fig. 3a, that

$$\mathbf{AC} = a - 1, \tag{18}$$

$$d = \sqrt{(a\cos s - x)^2 + (a\sin s - y)^2}. \tag{19}$$

The extension of the spring due to deformation, Z, can be expressed as

$$Z = \mathbf{BC} - \mathbf{AC} = d - a + 1, \tag{20}$$

Recalling Eq. (3), the spring force, per unit area per unit elemental length, due to deformation is given by

$$F(Z) = k_1 Z + k_2 g(Z), \tag{21}$$

and acts along $\vec{\mathbf{BC}}$. It can be projected into the tangential and normal directions giving q_t, q_n as follows

$$\begin{aligned}q_t &= F(Z)\cos(\theta - \gamma) \\ &= \frac{F(Z)}{d}[\cos\theta(a\cos s - x) + \sin\theta(a\sin s - y)]\end{aligned} \tag{22}$$

$$\begin{aligned}q_n &= F(Z)\sin(\theta - \gamma) - P \\ &= \frac{F(Z)}{d}[\sin\theta(a\cos s - x) - \cos\theta(a\sin s - y)] - P,\end{aligned} \tag{23}$$

where

$$P = P_e - P_i - F_0, \tag{24}$$

and F_0 is the spring force, per unit area per unit length at the initial spring length $l_0 = a - 1$. When $k_1 = k_2 = 0, F(Z) = 0$ and (16) reduces to

$$\begin{aligned}&\left[1 + \hat{\beta}|\theta'|\right]\theta'\theta'''' - \left[\theta'' + \hat{\beta}|\theta'|\theta'' - 3\hat{\beta}\theta' sign(\theta')\theta''\right]\theta''' \\ &+ \left[(\theta')^3 + p + \hat{\beta}|\theta'|(\theta')^3 - \hat{\beta} sign(\theta')\theta''^2 + 2\hat{\beta}\delta(\theta')\theta'\theta''^2\right]\theta'' = 0.\end{aligned} \tag{25}$$

In this case a simple linear solution $\theta = Cs + D$, where C, D are constants, is feasible. From the boundary conditions $\theta(0) = \frac{\pi}{2}, \theta\left(\frac{2\pi}{N}\right) = \frac{\pi}{2} + \frac{2\pi}{N}, C = 1, D = \frac{2\pi}{N}$, where N is the number of axes of symmetry. Substituting this solution into (17) then integrating gives the basic circular solution $x^2 + y^2 = 1$. With further simplification when $\hat{\beta} \to 0$, (25) is further reduced to the twice integrable case indicated in [3].

3. Bifurcation analysis

For small values of the pressure difference, the interior cylinder remains circular and the circular solution is unique. As the pressure difference increases beyond some critical value, non-circular solutions occur. These critical values of the pressure difference are called *bifurcation points* and their corresponding non-circular solutions are called *bifurcation solutions*. In this case, buckling solutions are sought of as solutions bifurcating from the circular one and the pressure difference as the bifurcation parameter. Mathematically, bifurcation may occur only at pressure difference that correspond to a singular linearized problem about the circular solution. An additional complexity arises here due to the nonlinear stress-strain relation of the vessel's wall. This complexity manifests itself in the existence of the absolute value, sign function, and Dirac-Delta function in the equilibrium equations.

To linearize (16) about the circular solution, assume that ξ, η, and ζ are the variations in θ, x, and y from their respective values in the circular solution. In this regard, we write

$$\theta = s + \frac{\pi}{2} + \xi, \quad \theta' = 1 + \xi', \tag{26}$$

$$x = \cos s + \eta, \tag{27}$$

$$y = \sin s + \zeta. \tag{28}$$

Substituting (26)–(28) into (19) and (20) gives

$$d = a - 1 - \eta\cos s - \zeta\sin s, \tag{29}$$

$$Z = -\eta\cos s - \zeta\sin s. \tag{30}$$

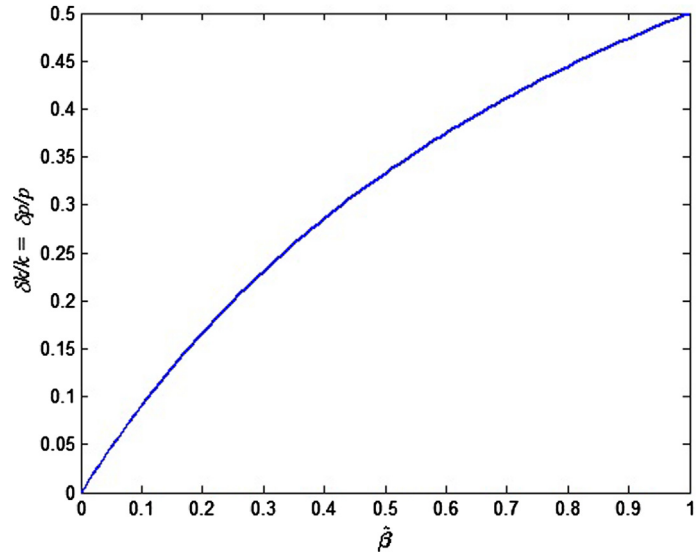

Fig. 4 Percentage of change in k and P due to nonlinearity.

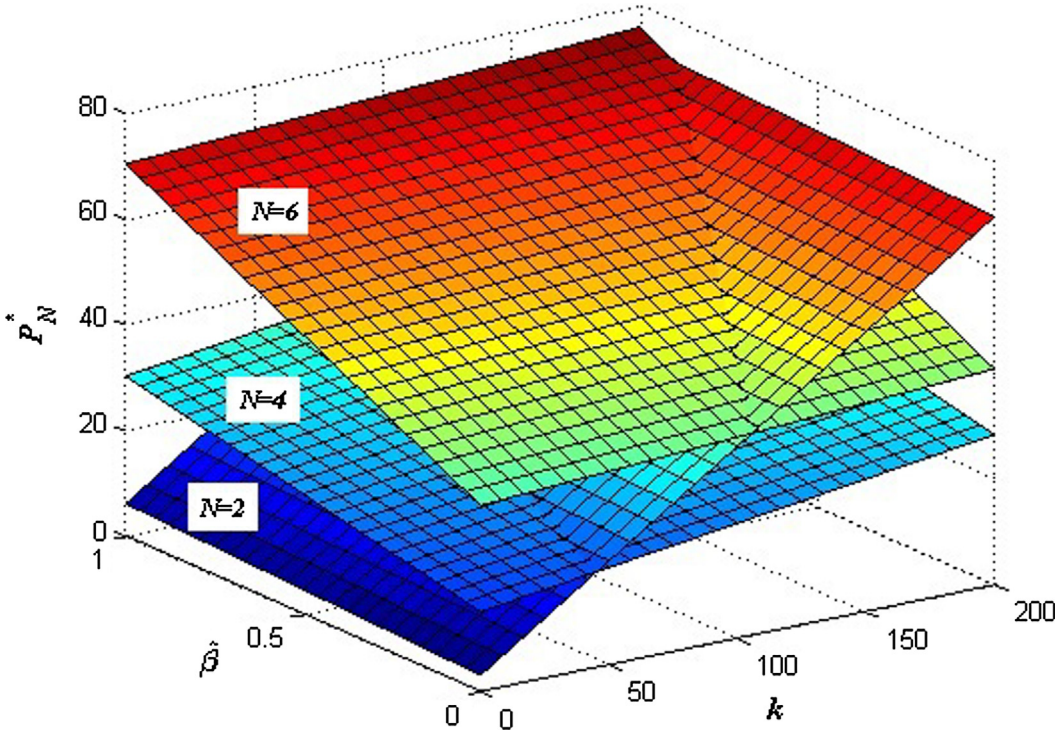

Fig. 5 Critical pressure difference vs k and $\hat{\beta}$ at $N = 2, 4, 6$.

Using (26)–(30) in linearizing (21)–(23) gives

$$F(Z) = -k_1(\eta\cos s + \zeta\sin s), \tag{31}$$

$$q_t = 0, \tag{32}$$

$$q_n = -k_1(\eta\cos s + \zeta\sin s) - P. \tag{33}$$

For small deformations close to the circular solution, θ' is slightly different than unity but still positive. Therefore, (16) becomes

$$\left(1+\hat{\beta}\right)\xi'''' + \left(1+\hat{\beta}+P\right)\xi'' - k_1\frac{d}{ds}(\eta\cos s + \zeta\sin s) = 0, \tag{34}$$

which upon dividing by $1+\hat{\beta}$ becomes

$$\xi'''' + \left(1+\frac{P}{1+\hat{\beta}}\right)\xi'' - \frac{k_1}{1+\hat{\beta}}\frac{d}{ds}(\eta\cos s + \zeta\sin s) = 0. \tag{35}$$

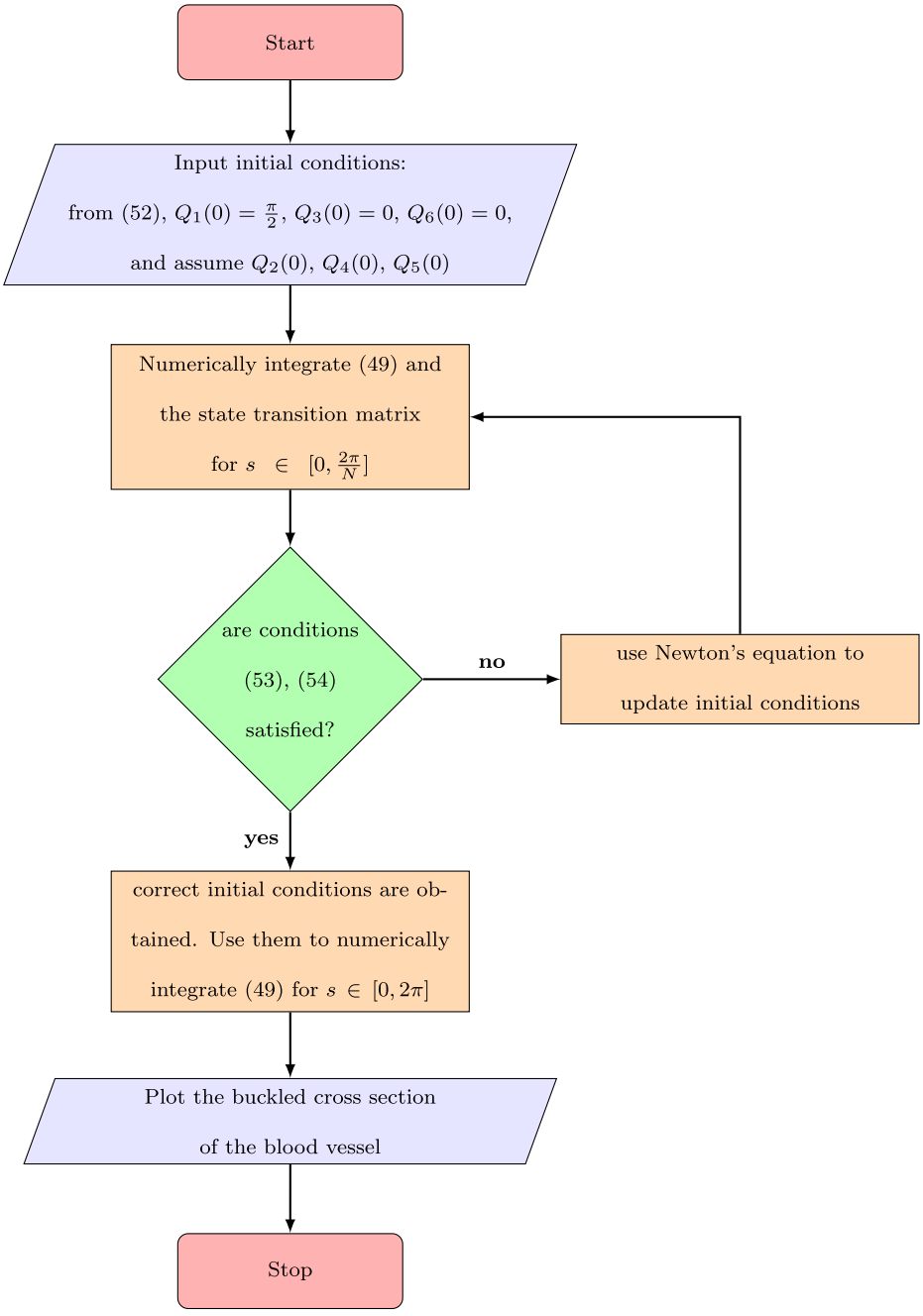

Fig. 6 A flow chart of the differential correction scheme used to obtain shapes of buckled cross section of a blood vessel.

We notice that the nonlinearity necessitates higher external pressure difference for buckling to occur. The percentages of change in the spring stiffness and external pressure difference due to nonlinearity are $\frac{\delta k}{k} = \frac{\delta P}{P} = \frac{\hat{\beta}}{1+\hat{\beta}}$. These percentages are plotted against $\hat{\beta}$ in Fig. 4 for $\hat{\beta} \in [0, 1)$.

Integrating (35) twice gives

$$\xi'' + \left(1 + \frac{P}{1+\hat{\beta}}\right)\xi - \frac{k_1}{1+\hat{\beta}} \int (\eta \cos s + \zeta \sin s) ds = c_1 s + c_2, \tag{36}$$

and using (17), the integration $\int (\eta \cos s + \zeta \sin s) ds$ in (36) can be carried out by parts to give

$$\xi'' + \left(1 + \frac{P}{1+\hat{\beta}}\right)\xi - \frac{k_1}{1+\hat{\beta}} (\eta \sin s - \zeta \cos s) = c_1 s + c_2. \tag{37}$$

The boundary conditions

$$\xi(0) = \xi''(0) = \zeta(0) = 0, \tag{38}$$

gives $c_2 = 0$. Noting that the variations should satisfy the boundary conditions and also give symmetrical shapes, they can be assumed as periodic functions vanish at the start and after a complete shape, i.e. variations should vanish at $s = \frac{2\pi}{N}$. The following trigonometric expansion is suitable

$$\xi(s) = \sum_{n=1}^{\infty} b_n \sin nNs \tag{39}$$

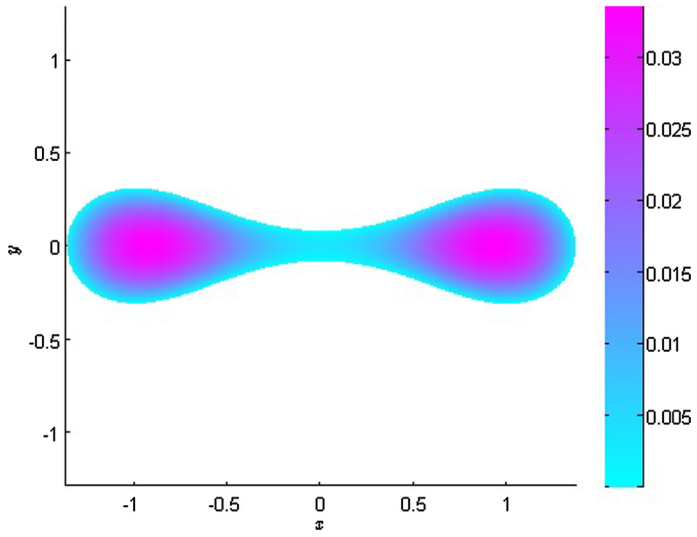

Fig. 7 Buckling cross section and blood velocity distribution for: $N = 2, \hat{\beta} = 0.05, P = 7.5$.

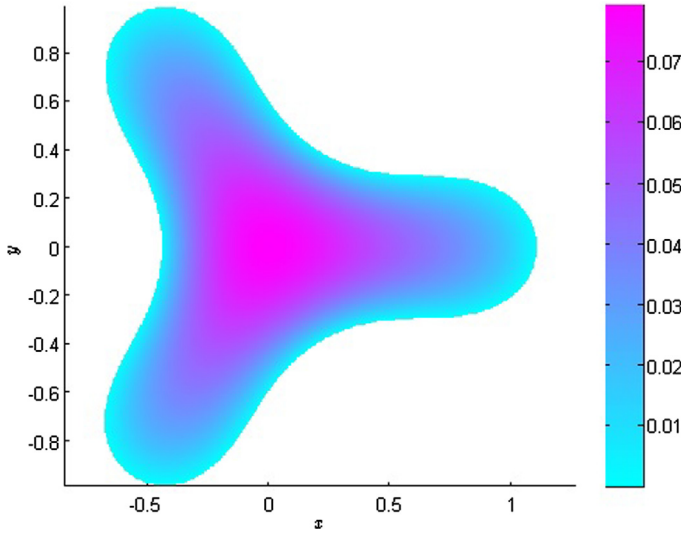

Fig. 8 Buckling cross section and blood velocity distribution for: $N = 3, \hat{\beta} = 0.05, P = 14$.

Substituting (26) into (17) and neglecting higher order terms of the variations we obtain linearized expressions for x' and y'. Comparing these expressions with the derivatives of (27) and (28) we obtain $\eta'(s)$ and $\zeta'(s)$, then integrating, we obtain the following expressions for the variations

$$\eta(s) = \sum_{n=1}^{\infty} \frac{b_n}{2} \left[\frac{\cos(nN+1)s}{nN+1} + \frac{\cos(nN-1)s}{nN-1} \right] + c_3, \tag{40}$$

$$\zeta(s) = \sum_{n=1}^{\infty} \frac{b_n}{2} \left[\frac{\sin(nN+1)s}{nN+1} - \frac{\sin(nN-1)s}{nN-1} \right] + c_4, \tag{41}$$

where c_3 and c_4 are constants. Knowing that $\eta(0) = 0$ gives $c_4 = 0$. Substituting (39)–(41) into (37) and evaluating at $s = \pi, s = 2\pi/N$ gives $c_1 = 0, c_3 = 0$ respectively, and one finally gets

$$\left[-n^2N^2 + \left(1 + \frac{P}{1+\hat{\beta}} \right) - \frac{k_1}{\left(1+\hat{\beta}\right)\left(n^2N^2-1\right)} \right] b_n = 0. \tag{42}$$

For $b_n \neq 0$ at any value of n, we must have

$$\left[-n^2N^2 + \left(1 + \frac{P}{1+\hat{\beta}} \right) - \frac{k_1}{\left(1+\hat{\beta}\right)\left(n^2N^2-1\right)} \right] = 0, \tag{43}$$

and the critical value for pressure difference P_N^* that satisfy this condition is given by

$$P_N^* = \left(1+\hat{\beta}\right)\left(n^2N^2-1\right) + \frac{k_1}{n^2N^2-1}. \tag{44}$$

For $\hat{\beta} = 0$, Eq. (44) gives the same results obtained by Wang in [3]. The change in the first critical pressure difference due to nonlinearity of the vessel's wall as compared with the linear wall is

$$\delta P_N^* = \hat{\beta}\left(N^2-1\right). \tag{45}$$

Eq. (45) indicates that the effect of wall nonlinearity on the critical pressure difference is not the same for all buckling

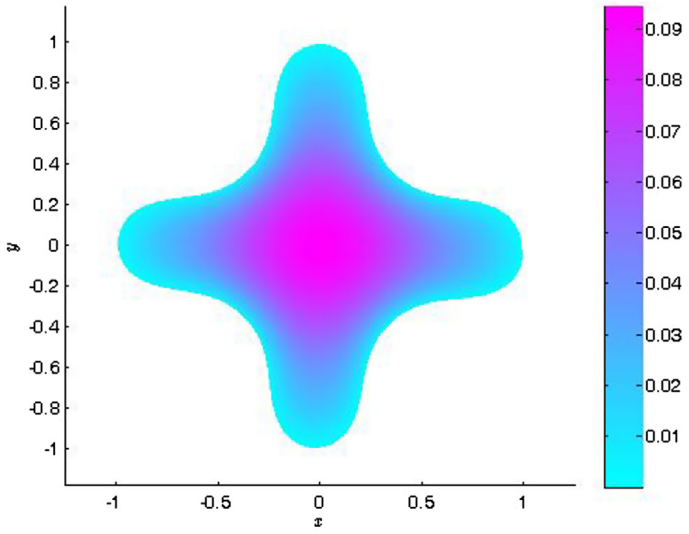

Fig. 9 Buckling cross section and blood velocity distribution for: $N = 4, \hat{\beta} = 0.05, P = 26.2$.

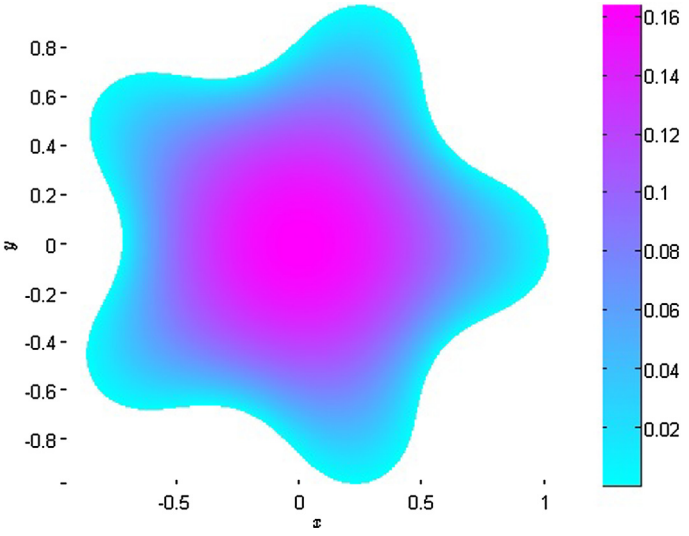

Fig. 10 Buckling cross section and blood velocity distribution for: $N = 5, \hat{\beta} = 0.05, P = 33$.

shapes. For a given value of N the right hand side of (44) can be represented graphically by a surface $P_N^* = P_N^*\left(k_1, \hat{\beta}; N\right)$ shown in Fig. 5. The line of intersection of each two surfaces represents the values of P^* at which twoshapes with different number of axes of symmetry occur.

The line of intersection between two successive surfaces parameterized by $N-1, N$ respectively can be expressed as follows

$$\hat{\beta} = \left[\frac{1}{N(N^2-1)(N-2)}\right] k_1 - 1, \quad N > 2. \tag{46}$$

Similarly the line of intersection between the two surfaces $N, N+1$ can be expressed by the equation

$$\hat{\beta} = \left[\frac{1}{N(N^2-1)(N+2)}\right] k_1 - 1, \quad N > 1. \tag{47}$$

Values of the spring stiffness between two successive lines of intersections lie within the interval

$$\left(1+\hat{\beta}\right) N\left(N^2-1\right)(N-2) < k_1 < \left(1+\hat{\beta}\right) N\left(N^2-1\right)(N+2). \tag{48}$$

It is obvious from (48) that the wall's nonlinearity widens the interval between two successive lines of intersection.

4. Numerical algorithm

For numerical calculations, the equilibrium equations can be written as a vector nonlinear differential equation [16]

$$\frac{d\mathbf{Q}}{ds} = \mathbf{F}(\mathbf{Q}, P; k_1; k_2; a), \tag{49}$$

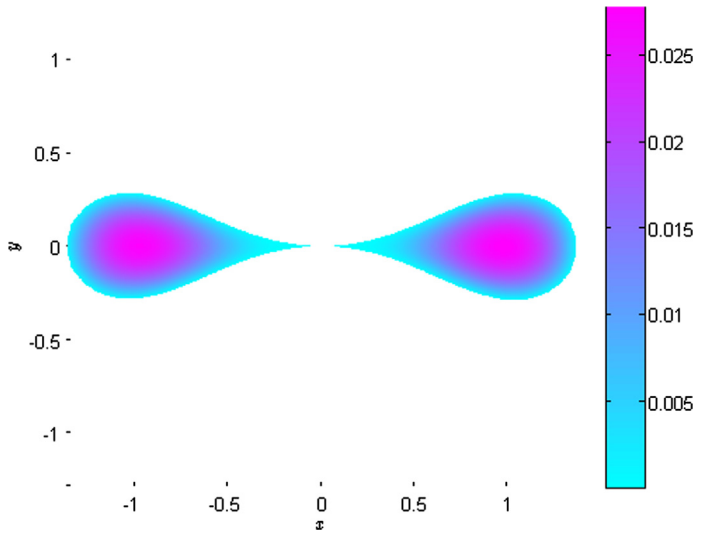

Fig. 11 Post buckling cross section and blood velocity distribution when opposite sides are in contact, $N = 2, \hat{\beta} = 0.05, P = 8.2, k_1 = 3, k_2 = 1$.

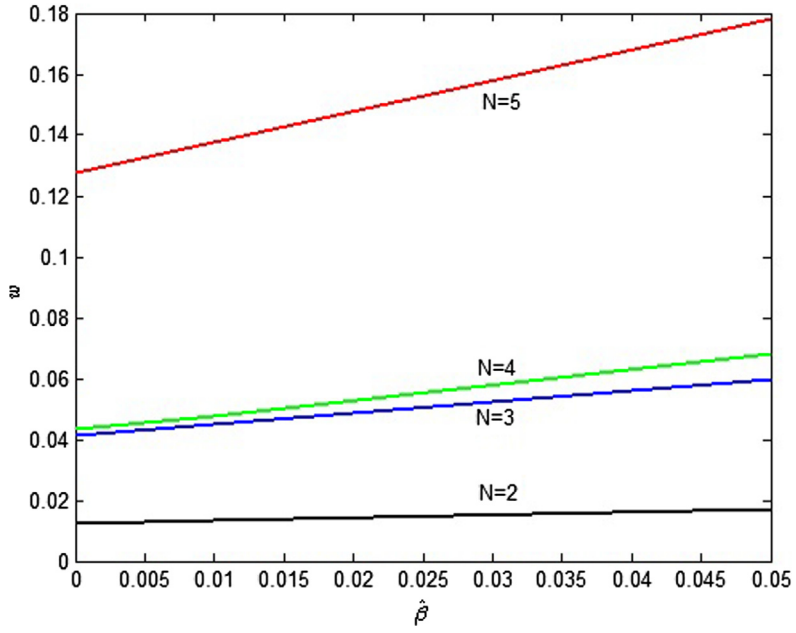

Fig. 12 Flow rate w Vs $\hat{\beta}$ at $N = 2, 3, 4, 5$.

where $\mathbf{Q}$ is the state vector and its elements are indicated as follows

$$\mathbf{Q}(s) = \begin{pmatrix} Q_1 \\ Q_2 \\ Q_3 \\ Q_4 \\ Q_5 \\ Q_6 \end{pmatrix} = \begin{pmatrix} \theta \\ \frac{d\theta}{ds} \\ \frac{d^2\theta}{ds^2} \\ T \\ x \\ y \end{pmatrix}, \tag{50}$$

In (50), the state variables are the local angle θ, its first and second derivatives, the tension T and the coordinates x, y. All states are assumed to be functions of the independent variable $s \in [0, 2\pi]$. While the pressure, the soft tissue stiffness, and the arbitrary distance a are the system parameters. By definition of $\mathbf{Q}$ we know that $Q_1' = Q_2, Q_2' = Q_3$, and from (14) and (15) we can obtain expressions for Q_3', Q_4', then from (17) we can obtain expressions for Q_5', Q_6'. Thus, the function $\mathbf{F}(\mathbf{Q}, P; k_1; k_2; a)$ will be

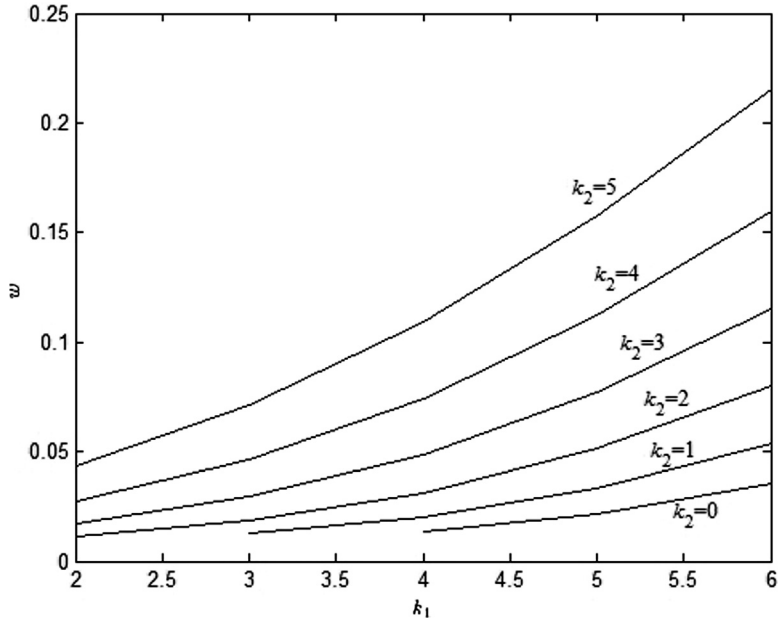

Fig. 13 Flow rate w Vs k_1 at $k_2 = 0, 1, 2, 3, 4, 5$ and $\hat{\beta} = 0, N = 2, P = 7.5$.

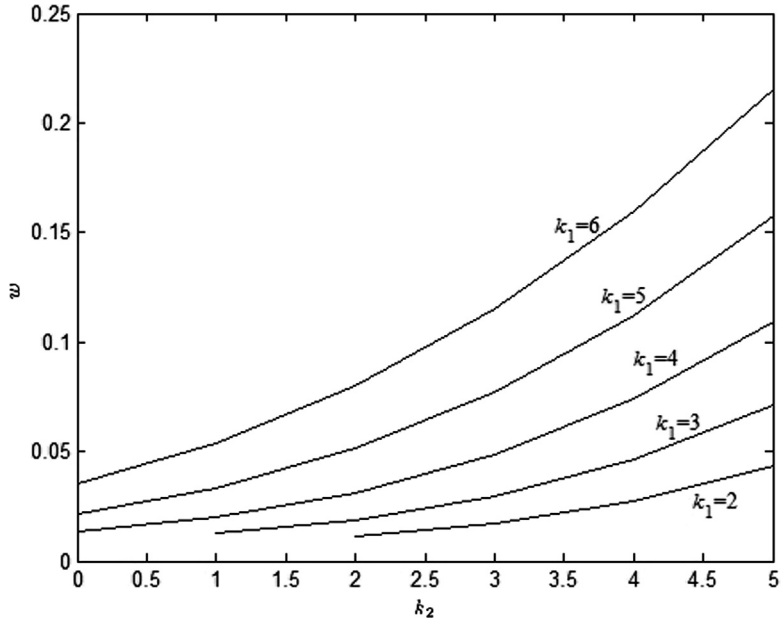

Fig. 14 Flow rate w Vs k_2 at $k_1 = 2, 3, 4, 5, 6$ and $\hat{\beta} = 0, N = 2, P = 7.5$.

$$\mathbf{F}(\mathbf{Q}, P; k_1; k_2; a) = \begin{pmatrix} Q_2 \\ Q_3 \\ \frac{Q_2 Q_4 - q_n - \hat{\beta} sign(Q_2) Q_3^2}{1+\hat{\beta}|Q2|} \\ -\left(1+\hat{\beta}|Q2|\right) Q_2 Q_3 - q_t \\ \cos Q_1 \\ \sin Q_1 \end{pmatrix}, \tag{51}$$

with the boundary conditions

$$Q_1(0) = \frac{\pi}{2}, \quad Q_3(0) = (0), \quad Q_6(0) = 0. \tag{52}$$

Seeking buckling solutions with symmetrical shapes, the states should satisfy the periodicity conditions of the buckled cross sections with number of axes of symmetry N. These periodicity conditions are represented as follows

$$Q_1\left(\frac{2\pi}{N}\right) = \frac{\pi}{2} + \frac{2\pi}{N}, \quad Q_3\left(\frac{2\pi}{N}\right) = 0, \tag{53}$$

$$Q_5^2(0) + Q_6^2(0) = Q_5^2\left(\frac{2\pi}{N}\right) + Q_6^2\left(\frac{2\pi}{N}\right), \tag{54}$$

An iterative differential correction scheme, is used to solve the nonlinear boundary value problem (49), (52)–(54) numerically.. The steps of the numerical integration scheme is repre-

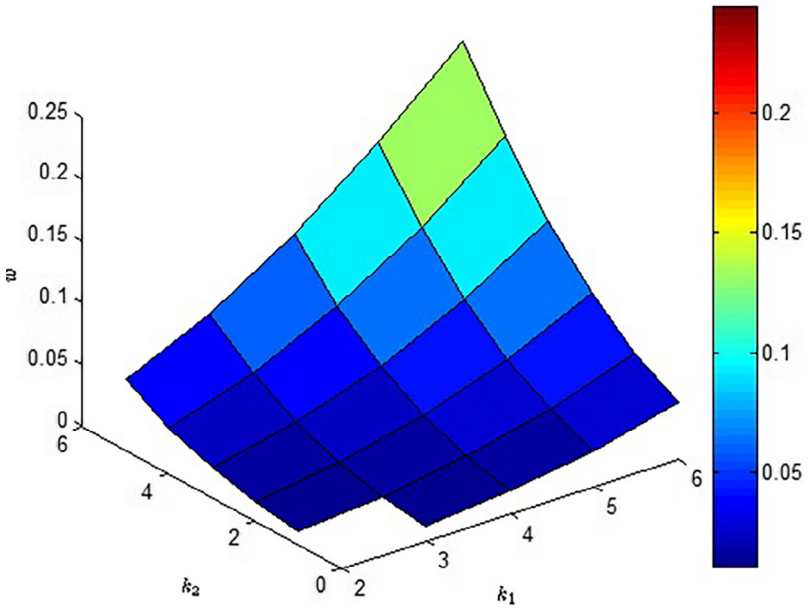

Fig. 15 Flow rate w Vs k_1, k_2 at $\hat{\beta} = 0, N = 2, P = 7.5$.

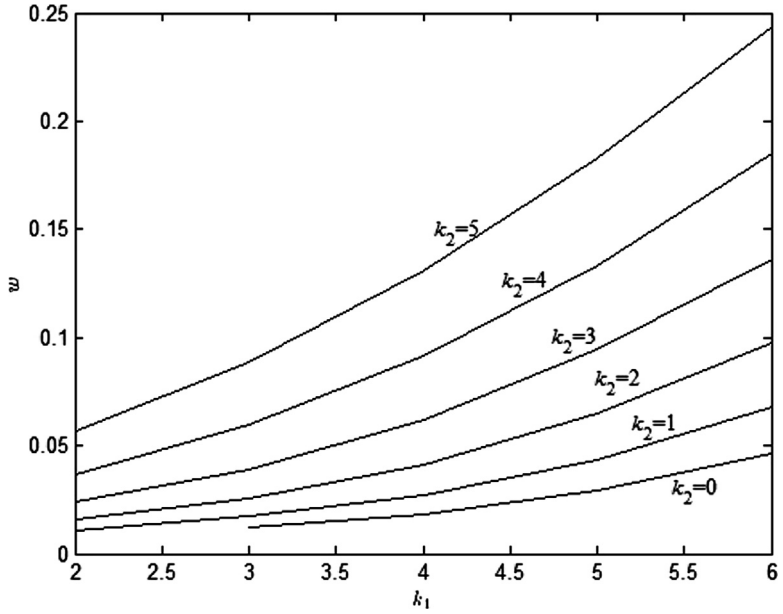

Fig. 16 Flow rate w Vs k_1 at $k_2 = 0, 1, 2, 3, 4, 5$ and $\hat{\beta} = 0.05, N = 2, P = 7.5$.

sented by the flow chart in Fig. 6, and for more details the reader is referred to [22,23]. In this scheme, assume $k_1, k_2, \hat{\beta}$, and P are known, an arbitrary set of values for $Q_2(0), Q_4(0), Q_5(0)$ are assumed. These values with those in (52) constitute the initial conditions used to numerically integrate the state equations, together with the associated differential equation of the state transition matrix. If, at the end of the domain of integration, the target conditions (53) and (54) are satisfied the process is terminated, and the assumed initial conditions are the correct ones. Otherwise, the Newton's equation is applied to update the initial conditions and the integration process is started again. Since a buckling shape has $N \geqslant 2$ symmetrical circumferential waves, the integration may be carried out only for $s \in \left[0, \frac{2\pi}{N}\right]$.

To validate the results of the differential correction scheme, the correct set of initial conditions at certain N are used again to numerically integrate the state Eqs. (49) only but this time for the whole domain $s \in [0, 2\pi]$. The plotted shapes, in this case, should have N number of axes of symmetry and satisfies periodicity conditions at $s = 2\pi$.

5. Results and discussion

Figs. 7–10 show the post buckling cross sections of a blood vessel for N = 2,3,4, and 5 respectively. These cross sections are calculated using the aforementioned scheme and introduced first in [16]. But, in the current study the velocity distribution of blood in these cross sections is calculated as well. The

values of the soft tissue constants are taken as $k_1 = 3, k_2 = 1$ and the vessel's wall nonlinearity $\hat{\beta} = 0.05$.

In these figures, the normalized Poisson's equation $\Delta v = -1$ is solved to obtain the velocity distribution $v(x, y)$ of the blood over the given cross section. We assumed that the blood interface with the vessel's wall extends to the entire surface so that the condition $v(x, y) = 0$ applies to all points (x, y) on the boundaries. This condition also applies after the deformation of the cross section.

The blood flow rate through each of the deformed shapes is calculated assuming the blood to be Newtonian. This is a good approximation for blood flow through vessels with large diameter. Having the velocity calculated at all points in the cross section of the blood vessel, by integrating the velocity on this cross section we obtain the blood flow rate [3–5,24]. Generally, The flow rate depends on the geometry of the cross section and the pressure drop along the vessel, as well as some other parameters. But, locally, we consider, the flow rate as a function of the cross-sectional geometry which depends on the pressure difference through the vessel's wall, the wall's stress strain characteristics, and the stiffness of the soft tissue.

We notice that for $N = 2$ when increasing the pressure difference on the vessel's wall to $P = 8.2$, keeping $\hat{\beta} = 0.05, k_1 = 3, k_2 = 1$, the two opposite sides of the vessel come into contact as shown in Fig. 11. For pressure difference P beyond this critical value, our formulation becomes invalid and a new formulation is required [4]. It is interesting to note that in the case of contact, if $\hat{\beta} = 0$, the solution doesn't converge into a symmetrical shape. The nonlinearity then helps the blood vessel to maintain the two capillary-like shape allowing blood to flow through it. Further more, in case if $\hat{\beta} \neq 0$ a pressure difference, lower than that in the linear mode, is required for contact between the two opposite sides to occur. In this analysis, we are able to predict the point of contact for $\hat{\beta} \neq 0$, but our model is not valid beyond the contact point.

5.1. Effect of wall nonlinearity on blood flow

In this study, we are emphasizing the effect of wall and soft tissue nonlinearities. Therefore, in Fig. 12 we show the relation between the blood flow rate w and the wall nonlinearity $\hat{\beta}$ at $N = 2, 3, 4$, and 5. Fig. 12 also indicates that the flow rate increases with $\hat{\beta}$ when keeping N, P, k_1, k_2 unchanged. This increase is more significant at higher number of axes of symmetry. As, at certain $\hat{\beta}$ when N increases the slope of the line $\hat{\beta}$ - w increases.

5.2. Effect of soft tissue nonlinearity on blood flow

It will be interesting to explore the effect of the nonlinearity of the surrounding soft tissue, represented by k_2, on the blood flow. However, we will let both k_1 and k_2 vary and calculate the flow rate keeping the other parameters unchanged. In the following figures, the value of k_2 starts from zero, while the value of k_1 starts from one. Fig. 13 shows the relation between the flow w and k_1 at different values of k_2 when $\hat{\beta} = 0, N = 2$, and $P = 7.5$. It is obvious that at certain value of k_2 the flow increases with k_1. Also the line represents the relation between w and k_1 is shifted upward and becomes more nonlinear when k_2 increases. This observation demonstrates the coupling between the effects of k_1 and k_2 on the blood flow.

Fig. 14 shows the relation between the flow w and k_2 at different values of k_1 when $\hat{\beta} = 0, N = 2$, and $P = 7.5$. The relation between w and k_2 is nonlinear and w increases with k_2. Their relation also is shifted upward at higher values of k_1.

Fig. 15 below shows three dimensional representation of the variation of the blood flow rate with k_1 and k_2 at $N = 2, P = 7.5$, and $\hat{\beta} = 0$.

In Figs. 16–18 we change $\hat{\beta}$ to 0.05 and study the effect of k_1, k_2 on the blood flow keeping $N = 2, P = 7.5$. Fig. 16 shows

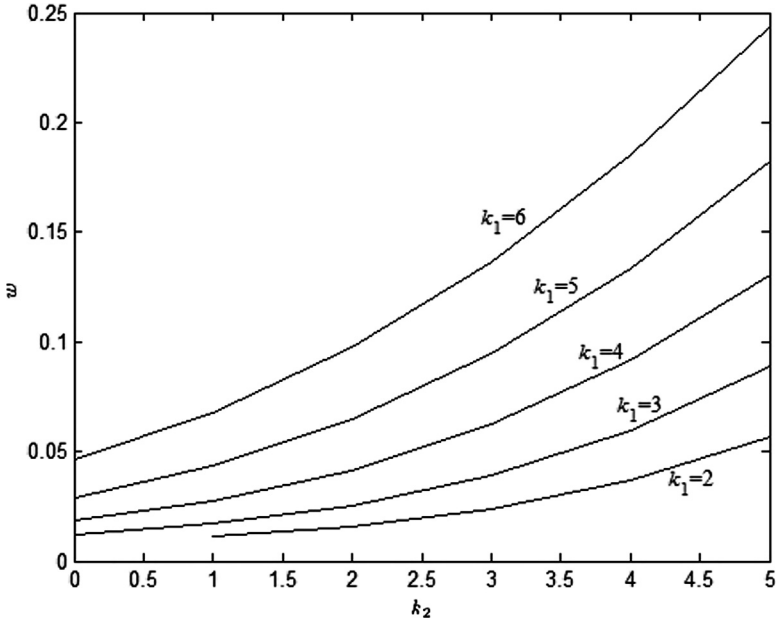

Fig. 17 Flow rate w Vs k_2 at $k_1 = 2, 3, 4, 5, 6$ and $\hat{\beta} = 0.05, N = 2, P = 7.5$.

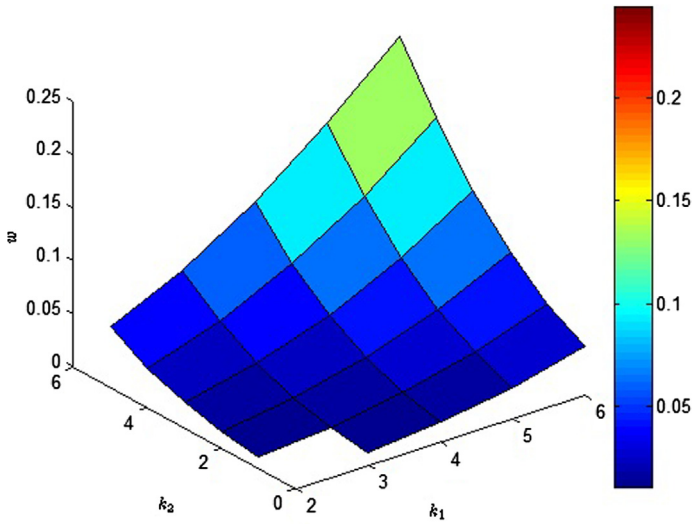

Fig. 18 Flow rate w Vs k_1, k_2 at $\hat{\beta} = 0.05, N = 2, P = 7.5$.

the relation between w and k_1 at different values of k_2 and Fig. 17 shows the relation between w and k_2 at different values of k_1 while Fig. 18 shows a three dimensional plot of w with k_1 and k_2 respectively.

In Figs. 16–18, the general behavior is the same as in Figs. 13–15. However, by comparing the two sets of figures the flow rate values when $\hat{\beta} = 0.05$ are higher than when $\hat{\beta} = 0$ at the same values of k_1 and k_2. This observation shows that the vessel's wall nonlinearity increases the effect of soft tissue nonlinearity on the blood flow but doesn't change the behavior of this effect. Also the $3D$ surfaces (15) and (18) still maintain their convex shapes with increasing $\hat{\beta}$. This indicates that measurements of the blood pressure, the shape, and the flow rate using medical devices can be used to estimate the elasticity parameters k_1 and k_2 uniquely, using some minimizing techniques. In a future study we plan to consider the case when the blood flow is taken as non-Newtonian shear-thinning fluid, in which case viscosity decreases with increasing the stresses [25]. Some other properties of blood can also be included into the analytical and numerical investigations. For example treating the blood as a suspension and studying the effect of nano-particles on its flow behavior [26,27].

6. Conclusion

The nonlinearity of blood vessel's walls affects their post-buckling shapes and blood flow rates. In this case, the critical pressure differences for buckled shapes can still be obtained analytically by linearizing the equilibrium equations. The post-buckling shapes can be calculated numerically by applying Newton's method to solve the corresponding full nonlinear boundary value problem. The blood flow rates through these blood vessels are found to increase with the nonlinearities. Our results show that even at small strains, the buckling and post-buckling shapes of the blood vessels using nonlinear material model are quite different from the previous results based on linear models. Experimental data are found consistent with the model for the spring nonlinearity used in our simulations.Therefore, our results can provide insights into the true nonlinear phenomenon of blood vessels deformations and their associated blood flow rates.

Acknowledgments

This research is partially supported by the research office at Texas A&M University in Qatar.

References

[1] J.B. Grotberg, O.E. Jensen, Biofluid mechanics in flexible tubes, Annu. Rev. Fluid Mech. 36 (2004) 12147.
[2] L.M. Kenneth, V. Nathur, D.A. Powell, Deformations and effects in isolated blood vessel testing, J. Biomech. Eng. 133 (1) (2011) 011005–011006.
[3] C.Y. Wang, L.T. Watson, M.P. Kamat, Buckling, Postbuckling, and flow rate through a tethered elastic cylinder under external pressure, J. Appl. Mech. 50 (1983) 13–18.
[4] J. Flaherty, J. Keller, S. Rubinow, Post buckling behavior of elastic tubes and rings with opposite sides in contacts, SIAM J. Appl. Math 23 (4) (1972) 446–455.
[5] S. Rubinow, J. Keller, Flow of a viscous fluid through an elastic tube with applications to blood flow, J. Theor. Biol. 23 (1972) 299–313.
[6] J. Holt, Flow of liquids through collapsible tubes, Circ. Res. 7 (1959) 342–353.
[7] T. Pedly, B. Brook, R. Seymour, Blood pressure and flow rate in the giraffe jugular vein, Philos. Trans.: Biol. Sci. 351 (1342) (1996) 855–866.
[8] H. Han, Determination of the critical buckling pressure of blood vessels using the energy approach, Ann. Biomed. Eng. (3) (2011) 1032–1040.
[9] R.P. Vito, S.A. Dixon, Blood vessel constitutive models-1995-2002, Annu. Rev. Biomed. Eng. (1) (2003) , 413–439.
[10] D.H. Bergel, The properties of blood vessels, in: Biomechanics, Its Foundations and Objectives, Prentice-Hall, Englewood Cliffs, N.J, 1972.
[11] Y.C. Fung, Biomechanics, Mechanical Properties of Living Tissues, Springer-Berlag, 1990.
[12] Y.C. Fung, S.Q. Liu, J.B. Zhou, Remodeling of the constitutive equation while a blood vessel remodels itself under stress, J. Biomech. Eng. 115 (1993) 453–459.

[13] A.C. Guyton, J.E. Hall, Textbook of Medical Physiology, Saunders Company, 1996.
[14] A.H. Moreno, A.I. Katz, L.D. Gold, R.V. Reddy, Mechanics of distension of dog veins and other very thin-walled tubular structures, Circ. Res. 27 (1970) 1069–1080.
[15] H. Ryder, E. Mole, E. Ferris, The influence of the collapsibility of veins on venous pressure, including a new procedure for measuring tissue pressure, J. Clin. Invest. (3) (1944) 333–341.
[16] M. Elgindi, D. Wei, M. Ghazy, Post-buckling shapes of a blood vessel embedded in nonlinear soft tissue, APJES (1) (2015) 29–33.
[17] H. Han et al, Artery buckling: new phenotypes, models, and applications, Ann. Biomed. Eng. 41 (7) (2013) 1399–1410.
[18] J.R. Womersley, Method for the calculation of velocity, rate of flow and viscous drag in arteries when the pressure gradient is known, J. Physiol. 127 (1955) 553–563.
[19] K. Rohlf, G. Tenti, The role of the Womersley number in pulsatile blood flow a theoretical study of the Casson model, J. Biomech. 34 (2001) 141–148.
[20] A. Arani, A. Arani, R. kolahchi, Non-Newtonian pulsating blood flow-induced dynamic instability of visco-carotid artery within soft surrounding visco-tissue using differential cubature method, J. Mech. Eng. Sci. 229 (16) (2015) 3002–3012.
[21] M. Makhsous et al, Investigation of soft-tissue stiffness alteration in denervated human tissue using an ultrasound indentation system, J. Spinal Cord Med. 31 (1) (2008) 88–96.
[22] M. Ghazy, B. Newman, Solvability conditions at equilibrium points, in: AIAA/AAS Astrodynamics Specialist Conference, Toronto, Ontario, Canada, 2–5 August, 2010.
[23] J. Stoer, R. Bulirsch, Introduction to Numerical Analysis, Springer-Verlag, New York, 1980.
[24] M. Elgindi, D. Yen, C. Wang, Deformation of a thin-walled cylindrical tube submerged in a liquid, J. Fluids Struct. 6 (1992) 353–370.
[25] S. Nahar, S. Jeelani, E. Windhab, Influence of elastic tube deformation on flow behavior of a shear thinning fluid, Chem. Eng. Sci. 75 (2012) 445–455.
[26] M. Hajmohammadi, Assessment of a lubricant based nanofluid application in a rotary system, Energy Convers. Manage. 146 (2017) 78–86.
[27] M. Hajmohammadi, Cylindrical Couette flow and heat transfer properties of nanofluids; single-phase and two-phase analyses, J. Mol. Liq. 240 (2017) 45–55.